The effect of host glass on optical absorption and fluorescence of Nd^{3+} in $x Na_2O–(30-x)K_2O–70B_2O_3$ glasses

2003 J. Phys.: Condens. Matter 15 6715

(http://iopscience.iop.org/0953-8984/15/40/009)

INSTITUTE OF PHYSICS PUBLISHING JOURNAL OF PHYSICS: CONDENSED MATTER

J. Phys.: Condens. Matter **15** (2003) 6715–6730 PII: S0953-8984(03)65577-3

The effect of host glass on optical absorption and fluorescence of Nd^{3+} in xNa_2O–$(30-x)K_2O$–$70B_2O_3$ glasses

Y C Ratnakaram[1], R P Sreekanth Chakradhar[2], K P Ramesh[2,4], J L Rao[3] and J Ramakrishna[2]

[1] Department of Physics, Sri Venkateswara University P G Centre, Kavali-524201, India
[2] Department of Physics, Indian Institute of Sciences, Bangalore-560012, India
[3] Department of Physics, Sri Venkateswara University, Tirupathi-517502, India

E-mail: kpramesh@physics.iisc.ernet.in

Received 2 July 2003, in final form 22 August 2003
Published 26 September 2003
Online at stacks.iop.org/JPhysCM/15/6715

Abstract

The effect of host glass composition on the optical absorption and fluorescence spectra of Nd^{3+} has been studied in mixed alkali borate glasses of the type xNa_2O–$(30-x)K_2O$–$69.5B_2O_3$–$0.5Nd_2O_3$ ($x = 5, 10, 15, 20$ and 25). Various spectroscopic parameters such as Racah (E^1, E^2 and E^3), spin–orbit (ξ_{4f}) and configuration interaction (α, β) parameters have been calculated. The Judd–Ofelt intensity parameters (Ω_λ) have been calculated and the radiative transition probabilities (A_{rad}), radiative lifetimes (τ_r), branching ratios (β) and integrated absorption cross sections (Σ) have been obtained for certain excited states of the Nd^{3+} ion and are discussed with respect to x. From the fluorescence spectra, the effective fluorescence line widths ($\Delta\lambda_{eff}$) and stimulated emission cross sections (σ_p) have been obtained for the three transitions $^4F_{3/2} \rightarrow {}^4I_{9/2}$, $^4F_{3/2} \rightarrow {}^4I_{11/2}$ and $^4F_{3/2} \rightarrow {}^4I_{13/2}$ of Nd^{3+}. The stimulated emission cross section (σ_p) values are found to be in the range (2.0–4.8) $\times 10^{-20}$ cm^2 and they are large enough to indicate that the mixed alkali borate glasses could be potential laser host materials.

1. Introduction

There is currently a great deal of interest in glasses doped with trivalent rare earth ions as they might be suitable for use in lasers and devices for optical communications [1–4]. Nd^{3+} doped glasses (silicates, phosphates, tellurites, borates etc) have been successfully used as glass lasers [5–12]. The stimulated emission cross section (σ_p) for the Nd^{3+} laser transition at 1060 nm is large and this parameter can be adjusted to maximize the performance by changing

[4] Author to whom any correspondence should be addressed.

the glass matrix using different modifier ions. Large values of (3.0–5.0) $\times 10^{-20}$ cm^2 have been reported for σ_p for the $^4F_{3/2} \rightarrow {}^4I_{11/2}$ transition of Nd^{3+} in tellurite, phosphotellurite and chlorophosphate glasses [6]. σ_p values for Nd^{3+} in the oxide glasses are found to increase in the order silicates, aluminates, germanates, borates, tellurite, fluorophosphate and phosphate glasses [13].

Many physical properties of oxide glasses containing alkali oxide as a modifier show non-linear behaviour if the alkali ion is gradually replaced by another alkali ion, keeping the total alkali content constant. This non-linear behaviour as a function of relative alkali content is known as the mixed alkali effect (MAE), and is observed for properties associated with alkali ion movement such as electrical conductivity, ionic diffusion, dielectric relaxation and internal friction [14]. However, the MAE is not much studied in borate glasses. In particular, spectroscopic investigations are meagre and they would be important as well as useful to gain insight into the microscopic mechanisms responsible for the effect. Recent progress in understanding the MAE has been initiated by the development of the dynamic structure model [15, 16]. Based on the results of extended x-ray absorption fine structure (EXAFS) experiments [17, 18], it was suggested, on the basis of this model, that the two ions can create their own distinct local environments in the glass. For alkali borate glasses, abrupt property changes were observed near 15–20 mol% modified oxide [15]. This peculiar behaviour, referred to as the 'borate anomaly', was first explained in terms of the unique ability of boron to exist in two distinct coordination states, the trigonal and tetrahedral states. In the present work, the effect of mixed alkalis on the optical properties of Nd^{3+} (0.5 mol%) doped xNa$_2$O–(30 − x)K$_2$O–70B$_2$O$_3$ (where x = 5, 10, 15, 20 and 25) glasses is investigated and interesting features have been observed.

The absorption spectra of rare earth ions serve as a basis for understanding their radiative properties. The intensities of the transitions for the rare earth ions have been successfully estimated using the Judd–Ofelt theory [19, 20]. The theory defines a set of three intensity parameters Ω_t (t = 2, 4 and 6) which are sensitive to the environment of the rare earth ion. From these parameters, other optical properties like the radiative transition probability for spontaneous emission, the radiative lifetime of excited states and branching ratios can be estimated. In order to increase the laser efficiency of a particular transition, it is important to optimize the glass composition to maximize the stimulated emission cross section (which depends on the radiative transition probability) of that transition. By changing the relative proportion of the two alkali ions, substantial increases in the stimulated emission cross section have been achieved.

2. Experimental details

The glasses used in the present investigation were prepared in our laboratory by taking Analar grade starting materials M_2CO_3 (M = Na or K), H_3BO_3 and Nd_2O_3 (purity 99.99%). Appropriate quantities of these chemicals were weighed, mixed thoroughly, ground to a fine powder and then melted in a porcelain crucible in an electric furnace in air at 950 °C for about 30 min. The melt was stirred with a quartz rod in order to achieve a good homogeneity and it was also ensured that the melt was free from any gas bubbles. The melt was quenched in air by pouring it onto a polished porcelain plate and pressing it with another porcelain plate. Glass samples with a thickness of about 1 mm and diameter 1 cm were obtained. The glasses thus obtained were transparent and blue in colour. Special care was taken to see that these glass discs were not exposed to moisture by keeping them in liquid paraffin containers. Optically transparent glasses were selected for optical studies. The glass formation was confirmed by using x-ray diffraction, recorded with a Scintag USA diffractometer using copper Kα radiation.

Optical absorption measurements were made using a Hitachi U-3400 spectrophotometer in the wavelength range 300–1000 nm. Fluorescence measurements were made using a Midac-FT photoluminescence spectrophotometer at room temperature in the wavelength range 700–1500 nm. The densities of the samples were measured by Archimedes' principle using xylene as the immersion liquid. The refractive index of the glasses was measured using an Abbe refractometer. Using density, refractive index and average molecular weight of the glass, physical properties like rare earth ion concentration (N), molar volume (V), ionic radius (r_i), interionic distance (r_p) and field strength (F) were determined using standard formulae.

The variation of spectroscopic parameters like Racah (E^1, E^2, E^3), spin–orbit (ξ_{4f}) and configuration interaction (α), Judd–Ofelt intensity parameters (Ω_2, Ω_4 and Ω_6), radiative lifetimes (τ_R), branching ratios (β) and stimulated emission cross sections (σ_p) have been studied as a function of x in the glass matrix. High values for σ_p (comparable with those reported in the literature) point to the possibility of these glasses being suitable for laser applications as laser host materials.

3. Theory

3.1. Spectroscopic parameters

The electronic configuration in the ground state for Nd^{3+} is $4f^3$ and the 4f electrons are shielded by the surrounding $5s^25p^6$ electrons. Therefore, the 4f electrons are only weakly perturbed by the surrounding ligands and consequently the absorption bands of the rare earth ions are sharper than those of the transition metal ions. For rare earth ions, the spin–orbit interactions are much stronger than the crystal field interactions and consequently the measured band positions are only slightly affected by the environment.

The interactions primarily responsible for the free ion structure in trivalent rare earth ions are the Coulomb interaction and the coupling between their spin and orbital angular momenta which is a magnetic interaction. The methods of Racah [21] are used to calculate the electrostatic interaction matrix elements. Wybourne [22] has calculated appropriate electrostatic and spin–orbit parameters of $Nd^{3+}(f^3)$ configurations using the RS coupling scheme.

If the crystal field effects are taken into account one has to rediagonalize the matrices for the same rare earth ion substituted in different host materials. Wong [23] observed that the effect of the crystalline field on these parameters is small and therefore a Taylor series expansion of the intermediate coupling energy levels can be applied for rare earth ions. Thus, the energy levels for rare earth ions in any matrix can be calculated without having to rediagonalize the matrix. Using the observed band energies E_J, zero point energies E_{0J} and partial derivatives [24] and using Taylor series expansion [23], the correction factors ΔE^k, $\Delta\xi_{4f}$ and $\Delta\alpha$ are evaluated by the least squares fit method. From the known free ion parameters E^{k0}, ξ^0_{4f} and α^0, the parameters E^k, ξ_{4f} and α in the complex are determined. Using the correction factors ΔE^k, $\Delta\xi_{4f}$ and $\Delta\alpha$ values, E_{cal} values are obtained. The method of calculating various spectroscopic parameters (E^1, E^2, E^3, ξ_{4f} and α), experimental and calculated transition energies has been described in our earlier papers [25, 26].

3.2. Spectral intensities—the Judd–Ofelt theory

The intensity of an absorption band is expressed in terms of a quantity called the 'oscillator strength'. The experimental oscillator strength (f_{exp}) was calculated as described in [26]. In the present work the intensities of all the absorption bands have been measured using the

area method. The uncertainties in the measurement of experimental oscillator strengths were estimated to be ±5% for intense transitions and ±10% for weak transitions. We used the Judd–Ofelt [19, 20] theory for data analysis. According to the Judd–Ofelt theory [19, 20], the oscillator strength of a transition between an initial J manifold $(S, L)J$ and a final J' manifold $(S', L')J'$ is given by

$$f_{\mathrm{cal}}(aJ, bJ') = \sum_{\lambda=2,4,6} T_\lambda \nu |\langle (SL)J \| U^\lambda \| (S'L')J' \rangle|^2, \tag{1}$$

where ν is the mean energy of the transition and $\|U^\lambda\|^2$ represents the square of the reduced matrix elements of the unit tensor operator $\|U^\lambda\|$ connecting the initial and final states. The matrix elements are calculated in the intermediate coupling approximations. Because of the electrostatic shielding of the 4f electrons by the closed 5p shell electrons, the matrix elements of the unit tensor operator between two energy manifolds in a given rare earth ion do not vary significantly when it is incorporated in different hosts. Therefore, the squared reduced matrix elements of the unit tensor operator $\|U^\lambda\|^2$ are taken from the literature [26].

Substituting the 'f_{exp}' for 'f_{cal}' and using the squared reduced matrix elements, T_λ parameters are obtained using least square fit method. The three intensity parameters Ω_2, Ω_4 and Ω_6, which are characteristic of a given rare earth ion in a given matrix, are obtained from

$$\Omega_\lambda = (2J+1)T_\lambda \left[9.218 \times 10^{-12} \times \frac{9n}{(n^2+2)^2} \right]. \tag{2}$$

From these Ω_λ parameters, radiative transition probabilities (A), radiative lifetimes (τ_{R}), branching ratios (β) and the integrated absorption cross section (Σ) have been calculated. Details of the necessary theory to describe the above can be found in the litera- ture [19–33].

3.3. Fluorescence

Good laser transitions are characterized by large cross sections for stimulated emission. The Judd–Ofelt theory can successfully account for the induced emission cross sections that are observed. The peak stimulated emission cross section $\sigma(\lambda_{\mathrm{p}})$ is related to the radiative transition probability $A(aJ, bJ')$ by

$$\sigma(\lambda_{\mathrm{p}}) = \frac{\lambda_{\mathrm{p}}^4}{8\Pi c n^2 \Delta\lambda_{\mathrm{eff}}} A_{\mathrm{rad}}(aJ, bJ'), \tag{3}$$

where λ_{p} is the peak wavelength and $\Delta\lambda_{\mathrm{eff}}$ is the effective line width of the emission band. $\sigma(\lambda_{\mathrm{p}})$ depends on the intensity parameter Ω_λ, the band width $\Delta\lambda_{\mathrm{eff}}$ and the refractive index n. Both Ω_λ and $\Delta\lambda_{\mathrm{eff}}$ are affected by compositional changes. From equation (3), it can be seen that A_{rad} and hence the emission probability and cross section depend strongly on the refractive index n and hence can be different for different compositions (even if Ω_λ are comparable).

4. Results and discussion

4.1. Spectroscopic parameters

The optical absorption spectra of Nd^{3+} in the mixed alkali borate glasses containing different concentrations of Na_2O/K_2O are shown in figure 1. The experimental (E_{exp}) and calculated (E_{cal}) energies of all the excited levels of Nd^{3+} ion, using the method mentioned in section 3, are presented in table 1. The Racah (E^1, E^2 and E^3), spin–orbit ($\xi_{4\mathrm{f}}$) and configuration interaction (α, β) parameters obtained for different compositions are also presented in table 1.

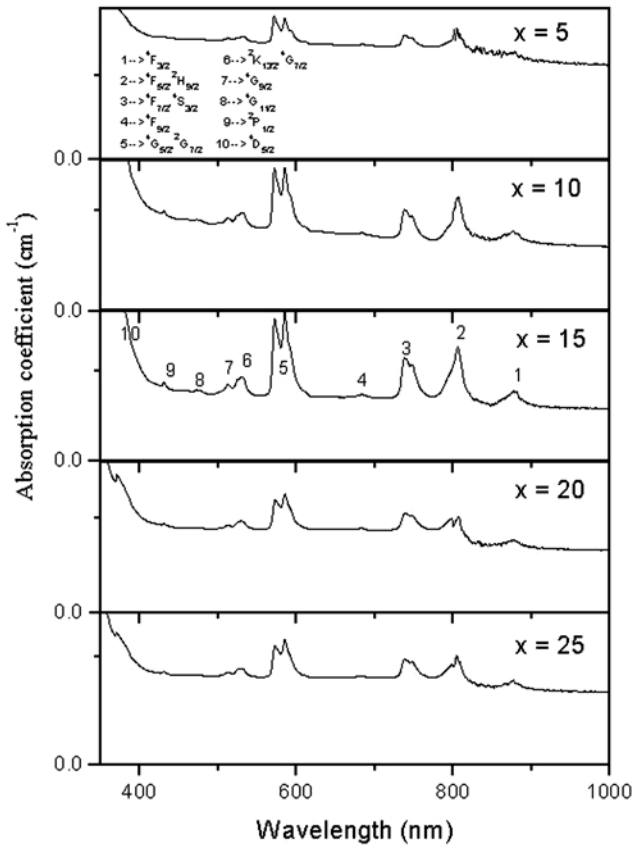

Figure 1. Optical absorption spectra of Nd^{3+} in $x Na_2O$–$(30 - x)K_2O$–$70B_2O_3$ ($x = 5$, 10, 15, 20 and 25) glasses.

The spin–orbit coupling parameter (ξ_{4f}) and configuration interaction parameter (α) decrease with increase of Na_2O content from 5 to 20 mol% and then increase for 25 mol% of Na_2O. The hydrogenic ratios E^1/E^3 and E^2/E^3, which indicate the radial properties of Nd^{3+}, are also presented in table 1. These values are more or less same for all the compositions, indicating that the radial properties of Nd^{3+} ion are not much affected by the changes in the relative alkali content.

The positions of $^{2S+1}L_J$ multiplets of Nd^{3+} ions are determined by the Racah and spin–orbit coupling parameters of the free ion. Changes in these positions in the glass arise from the nephelauxetic effect. Jorgensen [34] proposed that the nephelauxetic effect results from an expansion of the partly filled f-shell due to charge transfer from the ligands to the core of the central ion. The overlap with the ligands reduces the values of the free ion parameters and causes a contraction of the energy level structure of the ion in the glass. Consequently this leads to a shift of absorption and emission bands towards smaller energies. For example, in the case of binary sodium borate glasses, in the compositional range from 7.5 to 40 mol% of Na_2O, there is an overall shift of about 150 cm^{-1} of the peak position of the $^4I_{9/2} \rightarrow {}^4P_{1/2}$ transition to lower energy [35]. In the present work, there is no significant shift in the peak wavelengths either for the $^4I_{9/2} \rightarrow {}^4P_{1/2}$ transition or for the $^4I_{9/2} \rightarrow {}^4G_{5/2}$, $^2G_{7/2}$ (hypersensitive) transition with x, except for a small decrease of 15 cm^{-1} in the peak position of the hypersensitive transition for $x = 5$–10.

Table 1. Experimental (E_{exp}) and calculated (E_{cal}) energies and various spectroscopic parameters of Nd^{3+} in $x$$Na_2O$–$(30-x)K_2O$–$70B_2O_3$ ($x = 5$, 10, 15, 20 and 25) glasses at room temperature (energy values are in cm^{-1}).

Energy level	$x = 5$		$x = 10$		$x = 15$		$x = 20$		$x = 25$	
	E_{exp}	E_{cal}	E_{exp}	E_{cal}	E_{exp}	E_{cal}	E_{exp}	E_{cal}	E_{exp}	E_{cal}
$^4F_{3/2}$	11 367	11 343	11 393	11 358	11 354	11 355	11 367	11 357	11 399	11 361
$^4F_{5/2}$, $^2H_{9/2}$	12 411	12 456	12 380	12 465	12 403	12 454	12 388	12 453	12 411	12 476
$^4F_{7/2}$, $^4S_{3/2}$	13 528	13 450	13 537	13 463	13 537	13 452	13 546	13 455	13 533	13 483
$^4F_{9/2}$	14 605	14 805	14 637	14 810	14 626	14 795	14 626	14 798	14 626	14 837
$^4G_{5/2}$, $^2G_{7/2}$	17 074	17 133	17 089	17 135	17 089	17 124	17 089	17 128	17 089	17 149
$^2K_{13/2}$, $^4G_{7/2}$	18 845	18 877	18 845	18 882	18 862	18 895	18 898	18 931	18 880	18 925
$^4G_{9/2}$	19 487	19 398	19 507	19 418	19 488	19 409	19 507	19 429	19 583	19 467
$^2K_{15/2}$, $^2G_{9/2}$, $^2D_{3/2}$	21 158	21 037	21 180	21 055	21 158	21 045	21 158	21 066	21 135	21 110
$^4G_{11/2}$	21 804	21 743	21 780	21 724	21 733	21 689	21 733	21 684	21 828	21 761
$^2P_{1/2}$	23 222	23 188	23 222	23 188	23 222	23 188	23 222	23 189	23 222	23 181
$^4D_{5/2}$	28 604	28 676	28 563	28 658	28 604	28 639	28 604	28 653	28 604	28 658
Rms deviation	±119		±118		±103		±104		±116	
E^1	5038.5		5032.4		5036.6		5038.8		5026.9	
E^2	27.21		26.76		26.57		26.30		26.46	
E^3	488.0		487.7		487.4		487.6		488.2	
ξ_{4f}	939.3		934.1		928.7		926.3		937.8	
α	4.12		3.04		2.70		2.66		3.29	
E^1/E^3	10.32		10.31		10.33		10.33		10.29	
E^2/E^3	0.055		0.055		0.054		0.054		0.054	

4.2. Spectral intensities and intensity parameters

The experimental (f_{exp}) and calculated (f_{cal}) spectral intensities of different absorption bands of Nd^{3+} are presented in table 2. The rms deviations between the experimental and calculated spectral intensities is very low, confirming the validity of the Judd–Ofelt theory. The spectral intensities of all the transitions increase with x initially and exhibit a minimum around $x = 15$, some of the transitions exhibiting the feature more prominently. The Judd–Ofelt intensity parameters Ω_2, Ω_4 and Ω_6, which are obtained from the experimental oscillator strengths and using the equations given in section 2, are presented in table 3 along with those obtained in a few binary borate glasses. The intensity parameters are significantly enhanced in the mixed alkali borate glasses, as compared with those in the binary borate glasses. This indicates that the covalency increases when the third component is added to the glass matrix. Generally Ω_2 is an indicator of the covalency of the metal ligand bond and Ω_4 and Ω_6 parameters are related to the rigidity of the host matrix. In the present work, the Ω_2 parameter is low in glasses with $x = 5$ and high in glasses with $x = 20$. This indicates that the crystal field asymmetry at the site of the Nd^{3+} ion is low at $x = 5$ and high at $x = 20$. Variation of Ω_λ with x is also shown in figure 2.

4.2.1. Hypersensitive transition. For Nd^{3+} ions, $^4I_{9/2} \rightarrow {}^4G_{5/2} + {}^2G_{7/2}$ is the hypersensitive transition. This will follow the selection rules $\Delta J \leqslant 2$, $\Delta L \leqslant 2$ and $\Delta S = 0$. The intensity of the hypersensitive transition increases with the addition of Na_2O initially, goes through a shallow minimum when $x \approx 15$, and increases again with further addition of Na_2O before decreasing to the value of the binary potassium borate glass. This indicates structural changes

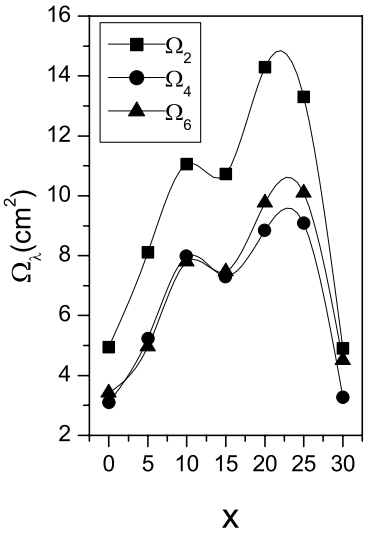

Figure 2. Variation of Judd–Ofelt intensity parameters ($\Omega_\lambda \times 10^{20}$) with x in the mixed alkali borate glasses.

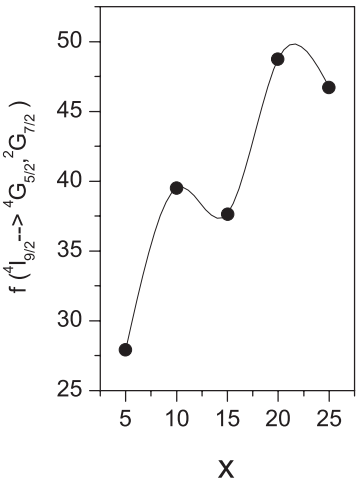

Figure 3. Variation of intensity of the hypersensitive transition ($f \times 10^6$) with x in the mixed alkali borate glasses.

Table 2. Experimental and calculated spectral intensities ($f \times 10^6$) of Nd^{3+} in $x Na_2O$–$(30 - x)K_2O$–$70B_2O_3$ ($x = 5$, 10, 15, 20 and 25) glasses at room temperature.

Energy level	$x = 5$		$x = 10$		$x = 15$		$x = 20$		$x = 25$	
	f_{exp}	f_{cal}	f_{exp}	f_{cal}	f_{exp}	f_{cal}	f_{exp}	f_{cal}	f_{exp}	f_{exp}
$^4F_{3/2}$	1.423	2.443	2.457	3.742	2.733	3.448	2.913	4.238	2.753	4.372
$^4F_{5/2}$, $^2H_{9/2}$	7.460	7.110	12.537	10.973	10.874	10.388	13.381	13.248	14.433	13.674
$^4F_{7/2}$, $^4S_{3/2}$	6.628	6.946	9.699	10.888	10.010	10.400	13.340	13.535	13.298	13.983
$^4F_{9/2}$	0.340	0.562	0.850	0.875	0.889	0.832	1.170	1.074	1.316	1.106
$^4G_{5/2}$, $^2G_{7/2}$	27.882	27.968	39.511	39.511	37.657	37.680	48.747	48.856	46.750	46.858
$^2K_{13/2}$, $^4G_{7/2}$	7.551	6.126	8.969	9.135	9.110	8.573	12.986	10.815	12.736	10.861
$^2K_{15/2}$, $^2G_{9/2}$, $^2D_{3/2}$	1.039	0.790	2.021	1.209	1.552	1.122	1.989	1.392	1.787	1.427
$^4G_{11/2}$	—	—	0.615	0.324	0.827	0.305	1.270	0.387	0.952	0.401
$^2P_{1/2}$	0.834	0.653	1.390	0.991	1.245	0.908	2.390	1.097	1.613	1.127
$^4D_{5/2}$	2.622	1.828	3.278	2.802	2.448	2.610	3.758	3.239	4.227	3.335
Rms deviation	±0.823		±0.975		±0.065		±1.171		±1.114	

that might have occurred at this composition. Figure 3 shows the variation of the intensity of the hypersensitive transition with x.

The initial increase in the intensity of the hypersensitive transition relative to the intensity in the binary system, indicates that the asymmetry around the Nd^{3+} ion increases with the addition of a second alkali. Since the covalency of the Nd–O bond has not changed much with x (as indicated by the absence of any shift of the wavelength of the hypersensitive transitions), the changes in the intensity of hypersensitive transition and the changes in Ω_λ are brought about by corresponding changes in $A_{S,P}$ (crystal field parameters). It has been proposed [36] that in oxide glasses a rare earth ion is surrounded by eight neighbouring oxygen atoms belonging to corners of the glass forming tetrahedra like BO_4, each octahedron donating two oxygen atoms

Table 3. Judd–Ofelt intensity parameters ($\Omega_\lambda \times 10^{20}$) ($cm^2$) and peak intensity ratios (I_L/I_S) of hypersensitive transition of Nd^{3+} in xNa_2O–$(30-x)K_2O$–$70B_2O_3$ ($x = 5$, 10, 15, 20 and 25) glasses at room temperature.

Glass matrix	Ω_2	Ω_4	Ω_6	I_L/I_S	References
$5Na_2O + 25K_2O + 70B_2O_3$	8.115	5.254	4.966	0.947	Present work
$10Na_2O + 20K_2O + 70B_2O_3$	11.064	7.977	7.799	1.000	Present work
$15Na_2O + 15K_2O + 70B_2O_3$	10.728	7.312	7.470	1.085	Present work
$20Na_2O + 10K_2O + 70B_2O_3$	14.295	8.835	9.761	1.107	Present work
$25Na_2O + 5K_2O + 70B_2O_3$	13.300	9.075	10.097	1.111	Present work
$30Na_2O + 70B_2O_3$	4.91	3.28	4.51		[40]
$30K_2O + 70B_2O_3$	4.94	3.10	3.42		[40]
$30PbO + 70B_2O_3$	3.96	3.77	4.88		[41]
$30Li_2O + 70B_2O_3$	4.20	3.89	4.74		[42]
$30Ca_2O + 70B_2O_3$	3.43	3.45	3.15		[42]

forming an edge of the cube. Addition of the second alkali, keeping the total alkali content constant, decreases the site symmetry around Nd^{3+}.

The hypersensitive transition in the absorption spectra of Nd^{3+} doped glasses is split into two peaks by the Stark splitting due to the crystal field and the peak to peak separation decreases with increasing x up to $x = 15$ (413 cm^{-1} for $x = 5$, 355 cm^{-1} for $x = 10$ and 330 cm^{-1} for $x = 15$ in the glass matrix) and afterwards there is no significant change in the peak-to-peak separation. The relative intensity ratio between the peaks I_L/I_S, where I_L is the intensity of the peak with longer wavelength and I_S is the intensity of the peak with shorter wavelength, increases with increase of the covalency of the Nd–O bond. The observed intensity ratios are presented in table 3. Variation of I_L/I_S with x is shown in figure 4. The spectral profile of the hypersensitive transition $^4I_{9/2} \rightarrow {}^4G_{5/2} + {}^2G_{7/2}$ is shown in figure 5 for all the glasses. The band structure consists of two clearly split peaks (1 and 2) and a weak feature (3) on the lower-energy side. As x increases from 5 to 25, the weak feature slowly disappears. Also the height (or absorbance value) of peak 1 (which is less than peak 2 for $x = 5$) increases and becomes greater than the height of peak 2 with increasing x, showing that structural changes occur in the glass matrix which affect the peak heights.

Judd [31] suggested that the appearance of the hypersensitive transition is strongly affected by changes in the symmetry of the crystalline field acting on the rare earth ion. In oxide glasses (like the present case) it has been proposed [36] that a rare earth is surrounded by eight oxygens belonging to the corners of BO_4 or any other glass-forming tetrahedra. In the present work, the hypersensitive profiles are different for different values of x up to $x = 15$, showing significant differences in crystal field asymmetries. On the other hand for $x = 20$ and 25 the hypersensitive profiles are similar. However, the $^4I_{9/2} \rightarrow {}^4F_{5/2}+{}^2H_{9/2}$ transition shows an observable splitting for $x = 20$ and 25 thus confirming that the crystal field asymmetry is different. Similar results have been observed by Gatterer *et al* [35] in the case of sodium borate and sodium silicate glasses.

4.3. Radiative transition probabilities and branching ratios

Electric dipole line strengths (S_{ed}), radiative transition probabilities (A_{rad}), branching ratios (β) and integrated absorption cross sections (Σ) for the excited states $^4G_{9/2}$, $^4G_{7/2}$, $^4G_{5/2}$, $^2H_{11/2}$, $^4F_{9/2}$, $^4F_{5/2}$ and $^4F_{3/2}$ of the Nd^{3+} ion have been calculated. These values are presented in table 4 for $x = 5$. Table 5 gives total radiative transition probabilities (A_T) and radiative lifetimes (τ_R) of all the above excited states in different compositions. The variation of A_T with x is shown

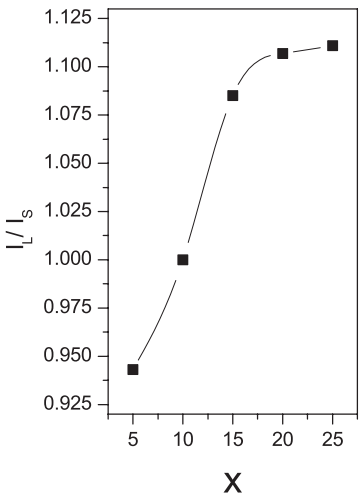

Figure 4. Variation of peak intensity ratios (I_L/I_S) with x in the mixed alkali borate glasses.

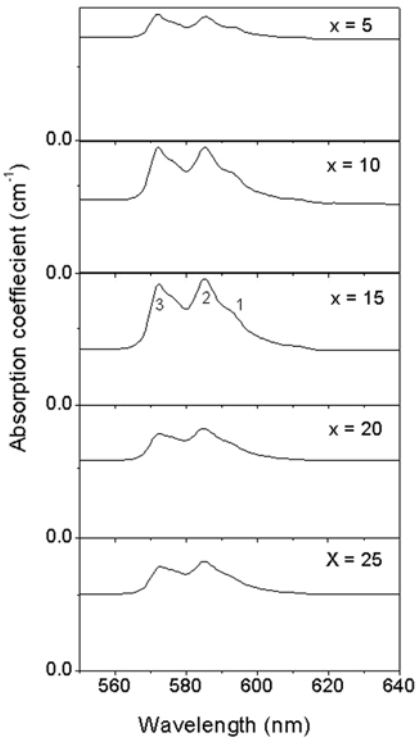

Figure 5. Variation of spectral profile of the hypersensitive transition ($^4F_{9/2} \rightarrow {}^4G_{5/2}$, $^2G_{7/2}$) with x in the mixed alkali borate glasses.

in figure 6 and it is similar to the variation of Ω_2, showing a shallow minimum at $x = 15$. Radiative lifetimes of all the excited states of the Nd^{3+} ion are greatest in the $x = 5$ glass and less for the other compositions. Branching ratios (β) and integrated absorption cross sections (Σ) of certain transitions which have large magnitudes are collected in table 6. From that table it is observed that the branching ratios of the transitions $^4G_{5/2} \rightarrow {}^4I_{9/2}$, $^4G_{7/2} \rightarrow {}^4I_{11/2}$ and $^4F_{5/2} \rightarrow {}^4I_{9/2}$ are higher when compared with the other transitions. The $^4F_{3/2} \rightarrow {}^4I_{11/2}$ transition is a potential lasing transition in the case of the Nd^{3+} ion. The calculated branching ratios of this transition are 0.468, 0.473, 0.478, 0.486 and 0.485 for $x = 5$, 10, 15, 20 and 25 respectively. Similar values ($\widetilde{=}0.5$) have been obtained for the branching ratios in other borate glasses [37–39] which are identified as potential laser host materials.

4.4. Emission spectra

The fluorescence spectra of Nd^{3+} in the wavelength range 6500–12 000 cm^{-1} under an excitation wavelength of 514 nm of the Ar^{3+} laser are shown in figure 7 for all the borate glasses studied. In the emission spectra of Nd^{3+}, a broad band at 11 360 cm^{-1}, a strong band at 9450 cm^{-1} and another band at 7520 cm^{-1} are identified. These bands are assigned to the transitions $^4F_{3/2} \rightarrow {}^4I_{9/2}$, $^4F_{3/2} \rightarrow {}^4I_{11/2}$ and $^4F_{3/2} \rightarrow {}^4I_{13/2}$ respectively. Of these three emission bands, the band at 9450 cm^{-1} is a potential lasing transition due to a large stimulated emission cross section. There is a small variation in peak wavelength (λ_P) for the transitions $^4F_{3/2} \rightarrow {}^4I_{9/2}$ (11 335–11 360 cm^{-1}) and $^4F_{3/2} \rightarrow {}^4I_{11/2}$ (9450–9435 cm^{-1}) with $x = 5$ and

Table 4. Electric dipole line strengths (S_{ed}), radiative transition probabilities (A_{rad}), branching ratios (β) and integrated absorption cross sections (Σ) of certain excited states of Nd^{3+} doped $5Na_2O$–$25K_2O$–$70B_2O_3$ glass.

Transition	Energy (cm^{-1})	S_{ed} (s^{-1})	A (s^{-1})	A_T (s^{-1})	β	Σ (cm^{-1})
$^4G_{9/2} \rightarrow {}^2K_{13/2}$	521	96.3	0	13 975	0	0
$^4G_{7/2}$	406	176.9	0		0	0
$^4G_{5/2}$	2 265	177.4	4.6		0	0.52
$^2G_{7/2}$	2 503	134.2	4.7		0	0.44
$^2H_{11/2}$	397	133.5	0		0	0
$^4F_{9/2}$	4 593	189.8	40.6		0.003	1.13
$^4F_{7/2}$	5 948	491.2	228.4		0.016	3.78
$^4S_{5/2}$	6 128	101.4	51.6		0.004	0.80
$^4F_{5/2}$	6 942	208.5	154.1		0.011	1.87
$^2H_{9/2}$	7 108	105.5	83.7		0.006	0.97
$^4F_{3/2}$	8 055	102.0	17.8		0.008	1.06
$^4I_{15/2}$	13 064	194.0	955.8		0.068	3.28
$^4I_{13/2}$	15 256	984.9	7 727.5		0.553	19.43
$^4I_{11/2}$	17 384	322.6	3 744.9		0.268	7.25
$^4I_{9/2}$	19 398	53.4	861.3		0.062	1.34
$^4G_{7/2} \rightarrow {}^4G_{5/2}$	1 859	154.0	2.7	13 490	0	0.46
$^2G_{7/2}$	2 097	69.6	1.8		0	0.24
$^2H_{11/2}$	2 197	61.9	1.8		0	0.22
$^4F_{9/2}$	4 187	11.3	2.3		0	0.08
$^4F_{7/2}$	5 542	181.4	85.0		0.006	1.62
$^4S_{3/2}$	5 722	108.0	55.7		0.004	1.00
$^4F_{5/2}$	6 536	268.3	206.2		0.015	2.82
$^2H_{9/2}$	6 702	252.8	209.5		0.016	2.73
$^4F_{3/2}$	7 649	119.2	146.9		0.011	1.47
$^4I_{15/2}$	12 658	16.6	92.7		0.007	0.34
$^4I_{13/2}$	14 850	56.9	1 414.5		0.105	3.75
$^4I_{11/2}$	16 978	603.8	8 135.2		0.603	16.51
$^4I_{9/2}$	18 992	166.3	3 136.3		0.232	5.09
$^4G_{5/2} \rightarrow {}^2G_{7/2}$	238	111.5	0	21 088	0	0
$^2H_{11/2}$	338	7.3	0		0	0
$^4F_{9/2}$	2 328	70.5	3.3		0	0.36
$^4F_{7/2}$	3 683	66.8	30.6		0.001	1.32
$^4S_{3/2}$	3 863	93.8	19.8		0.001	0.78
$^4F_{5/2}$	4 677	285.1	107.0		0.005	2.86
$^2H_{9/2}$	4 843	8.9	3.7		0	0.09
$^4F_{3/2}$	5 790	416.8	296.9		0.014	5.18
$^4I_{15/2}$	10 799	2.3	10.6		0.001	0.05
$^4I_{13/2}$	12 991	42.1	338.7		0.016	1.17
$^4I_{11/2}$	15 119	198.4	2 516.3		0.119	6.44
$^4I_{9/2}$	17 133	962.3	17 761.0		0.842	35.40
$^2H_{11/2} \rightarrow {}^4F_{9/2}$	1 990	91.9	1.3	519	0.003	0.19
$^4F_{7/2}$	3 345	99.3	6.8		0.013	0.36
$^4S_{3/2}$	3 525	30.4	2.4		0.005	0.11
$^4F_{5/2}$	4 339	13.4	2.0		0.004	0.06
$^2H_{9/2}$	4 505	194.5	32.6		0.063	0.94
$^4F_{3/2}$	5 452	4.1	1.2		0.002	0.02
$^4I_{15/2}$	10 461	141.0	296.2		0.570	1.58

Table 4. (Continued.)

Transition	Energy (cm^{-1})	S_{ed} (s^{-1})	A (s^{-1})	A_T (s^{-1})	β	Σ (cm^{-1})
$^4I_{13/2}$	12 653	13.8	51.3		0.099	0.19
$^4I_{11/2}$	14 781	11.5	68.1		0.131	0.18
$^4I_{9/2}$	16 795	6.6	57.4		0.111	0.12
$^4F_{9/2} \rightarrow {}^4F_{7/2}$	1 355	162.6	0.9	2 764	0	0.29
$^4S_{3/2}$	1 535	1.8	0		0	0
$^4F_{5/2}$	2 349	89.4	2.6		0.001	0.28
$^2H_{9/2}$	2 515	41.9	1.5		0.001	0.14
$^4F_{3/2}$	3 462	57.8	5.3		0.002	0.26
$^4I_{15/2}$	8 471	492.5	659.3		0.238	5.38
$^4I_{13/2}$	10 663	368.6	984.1		0.356	5.06
$^4I_{11/2}$	12 791	201.2	927.3		0.335	3.32
$^4I_{9/2}$	14 805	25.7	183.7		0.066	0.49
$^4F_{5/2} \rightarrow {}^2H_{9/2}$	166	23.8	0	3 445	0	0
$^4F_{3/2}$	1 113	90.7	0.5		0	0.24
$^4I_{15/2}$	6 122	114.2	96.2		0.028	1.50
$^4I_{13/2}$	8 314	294.6	621.4		0.180	5.26
$^4I_{11/2}$	10 442	107.5	449.2		0.130	2.41
$^4I_{9/2}$	12 456	321.1	2277.7		0.661	8.59
$^4F_{3/2} \rightarrow {}^4I_{15/2}$	5 009	13.9	9.6	2 649	0.004	0.22
$^4I_{13/2}$	7 201	103.9	213.6		0.081	2.41
$^4I_{11/2}$	9 329	277.5	1240.5		0.468	8.34
$^4I_{9/2}$	11 343	147.5	1185.3		0.447	5.39

Table 5. Total radiative transition probabilities (A_T) (s^{-1}) and radiative lifetimes (τ_R) (μs) of certain excited states of Nd^{3+} in xNa_2O–$(30-x)K_2O$–$70B_2O_3$ ($x = 5$, 10, 15, 20 and 25) glasses at room temperature.

Excited	$x = 5$		$x = 10$		$x = 15$		$x = 20$		$x = 25$	
level	A_T	τ_R	A_T	τ_R	A_T	τ_R	A_T	τ_R	A_T	τ_R
$^4G_{9/2}$	13 975	71.5	20 175	49.5	19 199	52.1	24 848	40.2	24 158	41.4
$^4G_{7/2}$	13 490	74.1	19 273	51.9	18 358	54.4	23 828	41.9	23 055	43.3
$^4G_{5/2}$	21 088	47.4	29 959	33.0	28 491	35.1	36 896	27.1	35 656	28.0
$^2H_{11/2}$	519	1925.6	733	1362.9	692	1445.1	881	1134.5	864	1157.2
$^4F_{9/2}$	2 764	361.7	4 334	230.7	4 114	243.1	5 291	188.9	5 441	183.7
$^4F_{5/2}$	3 445	290.2	5 362	186.0	5 044	198.0	6 399	156.2	6 604	151.4
$^4F_{3/2}$	2 649	377.1	4 123	242.5	3 876	258.0	4 898	204.0	5 022	199.0

10. There is no further change in the peak wavelengths for the other values of x. For the $^4F_{3/2} \rightarrow {}^4I_{13/2}$ transition, there is no change in the peak wavelength for any of the glasses, except that the energy decreases by 15 cm^{-1} for $x = 25$.

The observed fluorescence spectrum consists of overlapping lines arising from transitions between the crystal field split $^4F_{3/2}$ level and various sublevels of $^4I_{9/2}$, $^4I_{11/2}$ and $^4I_{13/2}$ states. The broad band at 11 360 cm^{-1} ($^4F_{3/2} \rightarrow {}^4I_{9/2}$) is composed of one main peak and accompanied by two small peaks at 10 895 and 11 025 cm^{-1}, while the sharp peak at 9450 cm^{-1}, i.e. the $^4F_{3/2} \rightarrow {}^4I_{11/2}$ band, is accompanied by three other sharp peaks at 8985, 9125 and 9305 cm^{-1}. The third one, which appears at 7525 cm^{-1}, is also composed of one main peak and three

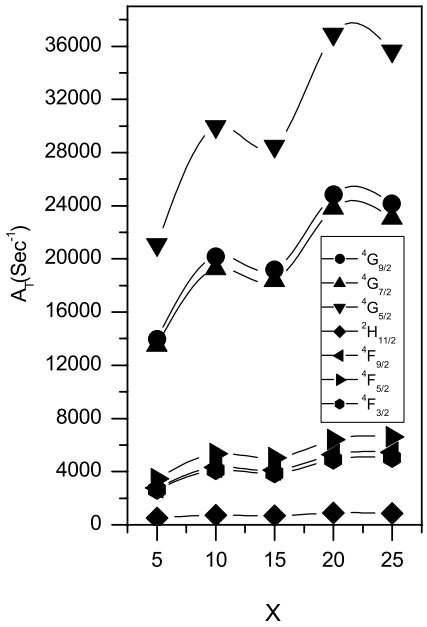

Figure 6. Variation of total radiative transition probabilities (A_T) with x in the mixed alkali borate glasses.

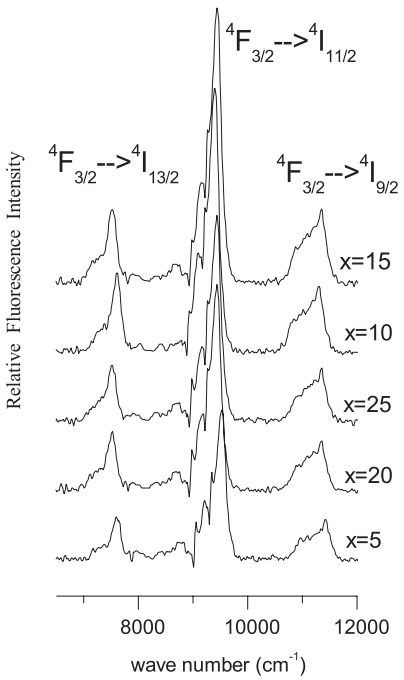

Figure 7. Fluorescence spectra of Nd^{3+} in xNa_2O–$(30 - x)K_2O$–$70B_2O_3$ ($x = 5$, 10, 15, 20 and 25) glasses.

small peaks at 7075, 7525 and 7255 cm^{-1}. All these peaks and their splitting are observed in the $x = 5$ glass. Similar splittings have also been observed for the remaining compositions.

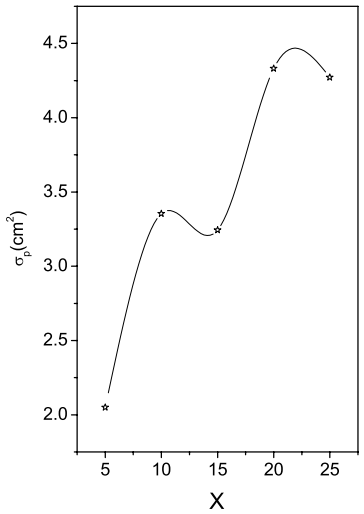

Figure 8. Variation of stimulated emission cross sections $(\sigma_p)(10^{-20})$ with x in the mixed alkali borate glasses.

Table 6. Branching ratios (β) and integrated absorption cross sections ($\Sigma \times 10^{18}$ cm^{-1}) of certain transitions of Nd^{3+} in xNa$_2$O–$(30-x)$K$_2$O–70B$_2$O$_3$ (x = 5, 10, 15, 20 and 25) glasses at room temperature.

	$x=5$		$x=10$		$x=15$		$x=20$		$x=25$	
Transition	β	Σ	β	Σ	β	Σ	β	Σ	β	Σ
$^4G_{9/2} \rightarrow {}^4I_{13/2}$	0.553	19.43	0.538	27.13	0.543	26.01	0.552	34.03	0.538	32.31
$^4G_{7/2} \rightarrow {}^4I_{11/2}$	0.603	16.51	0.585	22.13	0.592	22.00	0.603	29.07	0.587	27.33
$^4G_{5/2} \rightarrow {}^4I_{9/2}$	0.842	35.40	0.832	49.64	0.835	47.45	0.840	61.84	0.832	59.03
$^4F_{5/2} \rightarrow {}^4I_{9/2}$	0.661	8.59	0.660	13.32	0.659	12.55	0.660	15.94	0.664	16.48
$^4F_{3/2} \rightarrow {}^4I_{9/2}$	0.447	5.39	0.441	8.24	0.433	7.62	0.421	9.36	0.423	9.63
$^4F_{3/2} \rightarrow {}^4I_{11/2}$	0.468	8.34	0.473	13.02	0.478	12.34	0.486	15.84	0.486	16.31
$^4F_{3/2} \rightarrow {}^4I_{13/2}$	0.081	2.41	0.083	3.81	0.085	3.66	0.089	4.79	0.088	4.92
$^4F_{3/2} \rightarrow {}^4I_{15/2}$	0.004	0.22	0.004	0.36	0.004	0.34	0.004	0.45	0.004	0.46

The intensity of the sharp peak increases with x up to 15 and for $x > 15$ the intensity of the peak appears to decrease. All the smaller peaks were observed on the longer-wavelength side of each of the main peaks for all the glasses studied.

The intensity parameters obtained from the optical absorption spectra have been used to determine the radiative properties. Table 7 gives peak wavelength (λ_P), radiative transition probabilities (A_{rad}), effective band widths ($\Delta\lambda_{eff}$), stimulated emission cross sections (σ_p) and measured branching ratios (β) of the $^4F_{3/2} \rightarrow {}^4I_{13/2}$, $^4F_{3/2} \rightarrow {}^4I_{11/2}$ and $^4F_{3/2} \rightarrow {}^4I_{9/2}$ transitions. The emission band ($^4F_{3/2} \rightarrow {}^4I_{11/2}$) at 9450 cm^{-1} has been considered as a potential lasing transition due to the large stimulated emission cross section. An efficient laser transition is characterized by a large stimulated emission cross section. The stimulated emission cross-section σ_p, increases with increasing x, but for $x = 15$, σ_p values decrease again due to the mixed alkali effect. Variation of σ_P with different x values is shown in figure 8. The value of σ_p increases from 2.050×10^{-20} to 3.354×10^{-20} cm^2 for $x = 5$ and 10 and decreases to 3.243×10^{-20} cm^2 for $x = 15$. For $x = 20$ and 25, σ_p increases to 4.331×10^{-20} cm^2

Table 7. Certain radiative and fluorescence properties of Nd^{3+} in $x$$Na_2O$–$(30 - x)K_2O$–$70B_2O_3$ (x = 5, 10, 15, 20 and 25) glasses at room temperature.

	$^4F_{3/2} \rightarrow {}^4I_{9/2}$					$^4F_{3/2} \rightarrow {}^4I_{11/2}$					$^4F_{3/2} \rightarrow {}^4I_{13/2}$				
Glass x	λ_p (nm)	A_{rad} (s^{-1})	$\Delta\lambda$ (cm^{-1})	σ_p (10^{-20} cm^2)	β	λ_p (nm)	A_{rad} (s^{-1})	$\Delta\lambda$ (cm^{-1})	σ_p (10^{-20} cm^2)	β	λ_p (nm)	A_{rad} (s^{-1})	$\Delta\lambda$ (cm^{-1})	σ_p (10^{-20} cm^2)	β
5	882	1185	475	0.945	0.234	1058.2	1240	330	2.050	0.606	1329.7	213	309	0.594	0.159
10	881	1817	495	1.388	0.235	1059.8	1948	318	3.354	0.608	1329.7	341	272	1.081	0.157
15	881	1679	492	1.290	0.251	1059.8	1852	313	3.243	0.588	1329.7	330	321	0.885	0.160
20	881	2063	447	1.746	0.216	1059.8	2381	301	4.331	0.610	1329.7	434	300	1.242	0.172
25	881	2124	460	1.748	0.233	1059.8	2439	312	4.272	0.617	1332.4	439	276	1.371	0.149

Table 8. Certain physical properties of Nd^{3+} in $x Na_2O$–$(30 - x)K_2O$–$70B_2O_3$ ($x = 5$, 10, 15, 20 and 25) glasses at room temperature.

	x				
Property	5	10	15	20	25
Average molecular weight, M (g)	84.50	82.82	81.28	79.67	78.06
Density, d (g cm^{-3})	2.632	2.548	2.596	2.788	2.636
Refractive index, n	1.506	1.506	1.505	1.506	1.507
Concentration, $N \times 10^{-22}$ (ions cm^{-3})	0.938	0.925	0.962	1.054	1.017
Polaron radius, r_p (Å)	1.911	1.822	1.895	1.838	1.860
Interionic distance, r_i (Å)	4.741	4.763	4.702	4.561	4.615
Field strength, $F \times 10^{-16}$ (cm^2)	0.821	0.903	0.835	0.888	0.867

and decreases to 4.272×10^{-20} cm^2 respectively. The stimulated emission cross sections are higher in these mixed alkali borate glasses than in the other borate glasses. Of all these glasses, $x = 20$ (i.e. 20 mol% of Na_2O + 10 mol% of K_2O) gives the highest emission cross section. The physical properties described in section 2 of Nd^{3+} doped $x Na_2O$–$(30 - x)K_2O$–$70B_2O_3$ glasses are shown in table 8.

5. Conclusions

The Judd–Ofelt theory describes the spectral intensities of the transitions of Nd^{3+} in mixed alkali borate glasses quite well. The three Judd–Ofelt intensity parameters in the mixed alkali borate glasses are higher when compared with binary borate glasses. The higher value of the Ω_2 parameter is related to the higher covalency (low ionicity) between the neodymium cation and oxide anions and/or to a relatively low symmetry of the local surroundings of the neodymium ion. All three intensity parameters decrease at $x = 15$ mol% in the glass matrix due to structural variations. The intensity of the hypersensitive transition also shows a minimum at $x = 15$ in the glass matrix. From the shape of the profile of the hypersensitive transition, it is concluded that crystal field environment is different for different mixed alkali borate glasses.

The effect of mixed alkali elements on the radiative properties of Nd^{3+} in the borate glasses is investigated. The radiative transition probabilities, radiative lifetimes and branching ratios are calculated using intensity parameters obtained from the absorption spectra. Radiative lifetimes of all the excited states of Nd^{3+} decreased at $x = 15$ in the glass matrix (i.e. at equal mol% of sodium and potassium content). Branching ratios and integrated absorption cross sections are compared for certain transitions. From the fluorescence spectra, emission peak wavelengths, observed branching ratios and emission cross sections are reported for the three transitions $^4F_{3/2} \rightarrow {}^4I_{13/2}$, $^4F_{3/2} \rightarrow {}^4I_{11/2}$ and $^4F_{3/2} \rightarrow {}^4I_{9/2}$ of the Nd^{3+} ion. Of these three transitions $^4F_{3/2} \rightarrow {}^4I_{11/2}$ (9450 cm^{-1}) is a potential lasing transition. The stimulated emission cross section of the 9450 cm^{-1} band, i.e. $^4F_{3/2} \rightarrow {}^4I_{11/2}$ of Nd^{3+}, is large where $x = 20$ in the glass matrix. The large stimulated emission cross section in this glass suggests the possibility of utilizing this glass system as a laser material.

Acknowledgments

One of the authors (YCR) expresses his thanks to the Head of the Department of Physics, SVUPG centre, Kavali for his encouragement in the execution of the present work at the

Indian Institute of Sciences, Bangalore. RPSC thanks the Science and Engineering Research Council (SERC), Department of Science and Technology, New Delhi for the award of a Fast Track research project under the Young Scientist scheme.

References

[1] Dune B and Zink J I 1991 *J. Mater. Chem.* **1** 903
[2] Sanchez C, Lebeau B and Viana B 1994 *Sol–Gel Optics III* (*SPIE Proc. Series* vol 2288) ed J D Mackenzie (New York: SPIE) p 227
[3] Jacquier B, Linares C, Mahion R, Adam J L, Denoue E and Lucas J 1994 *J. Lumin.* **60/61** 175
[4] Hanna D C 1993 *Solid State Lasers* ed M Inguscio and R Wallenstein (New York: Plenum) p 231
[5] Reisfeld R and Jorgensen C K 1997 *Lasers and Excited States of Rare Earths* (Berlin: Springer)
[6] Weber M J, Mayers J D and Blackburn D H 1981 *J. Appl. Phys.* **52** 2944
[7] Pearson A D, Porto S P S and Northover W R 1993 *J. Appl. Phys.* **73** 8066
[8] Wang J, Reckie L, Brocklesby W S, Chow Y J and Payne D N 1995 *J. Non-Cryst. Solids* **180** 207
[9] Li H, Li L, Vienna J D, Qian M, Wang Z, Darab J G and Peelar D K 2000 *J. Non-Cryst. Solids* **278** 35
[10] Lu K and Dutta N K 2001 *J. Appl. Phys.* **89** 6
[11] Kumar G A, De la Rosa-Cruz E, Martinez A, Unnikrishnan N V and Ueda K 2002 *J. Phys. Chem. Solids* **64** 69
[12] Kumar G A, De la Rosa-Cruz E, Ueda K, Martinez A and Barbosa-Garcia O 2003 *Opt. Mater.* **22** 201
[13] Jacobs R R and Weber M J 1976 *IEEE J. Quantum Electron.* **12** 102
[14] Day D E 1976 *J. Non-Cryst. Solids* **21** 343
[15] Maass P, Bunde A and Ingram M D 1992 *Phys. Rev. Lett.* **68** 3064
[16] Bunde A, Ingram M D and Maass P 1994 *J. Non-Cryst. Solids* **72** 1222
[17] Greaves G N, Gurman S J, Catlow C R A, Chadwick A V, Honde-Walter S N, Henderson C M B and Dobson B R 1991 *Phil. Mag.* A **64** 1059
[18] Honde-Walter S N, Inman J M, Dent A J and Greaves G N 1993 *J. Phys. Chem.* **97** 9330
[19] Judd B R 1962 *Phys. Rev.* **127** 750
[20] Ofelt G S 1962 *J. Chem. Phys.* **37** 511
[21] Racah G 1942 *Phys. Rev.* **62** 438
[22] Wybourne B G 1960 *J. Chem. Phys.* **32** 639
[23] Wong E Y 1961 *J. Chem. Phys.* **35** 544
[24] Ratnakaram Y C 1987 *PhD Thesis* S V University, Tirupathi, India
[25] Ratnakaram Y C and Sudharani N 1997 *J. Non-Cryst. Solids* **217** 291
[26] Ratnakaram Y C and Reddy A V 2000 *J. Non-Cryst. Solids* **227** 142
[27] Carnall W T, Fields P R and Wybourne B G 1963 *J. Chem. Phys.* **42** 3797
[28] Jorgensen C K 1962 *Absorption Spectra and Chemical Bonding in Complexes* (Oxford: Pergamon)
[29] Reisfeld R 1975 *Structure and Bonding* (Berlin: Springer) p 22
[30] Jorgensen C K 1971 *Modern Aspects of Ligand Field Theory* (Amsterdam: North-Holland)
[31] Judd B R 1956 *Proc. Phys. Soc. Lond. Ser.* A **69** 157
[32] Carnall W T, Crosswhite H and CrossWhite H M 1977 Energy level structure and transition probabilities of trivalent lanthanides in LaF_3 *Argonne National Laboratory Report*
[33] Gschneider K A Jr and LeRoay E (ed) 1998 *Handbook on the Physics and Chemistry of Rare Earths* (New York: Elsevier) chapter 167
[34] Jorgensen C K 1962 *Prog. Inorg. Chem.* **4** 73
[35] Gatterer K, Pucker G, Fritzer H P and Arafa S 1994 *J. Non-Cryst. Solids* **176** 237
[36] Reisfeld R and Eckstein Y 1972 *J. Solid State Chem.* **5** 174
[37] Saisudha M B, Koteswara Rao K S R, Bhat H L and Ramakrishna J 1996 *J. Appl. Phys.* **80** 4845
[38] Pozza G, Azo D, Bettinelli M, Speghini A and Casarin M 1996 *Solid State Commun.* **97** 521
[39] Ratnakaram Y C and Buddudu S 1996 *Solid State Commun.* **97** 651
[40] Takebe H, Morinaga K and Izumitani T 1994 *J. Non-Cryst. Solids* **178** 58
[41] Saisudha M B and Ramakrishna J 1996 *Phys. Rev.* B **53** 6186
[42] Nachimuthu P, Harikrishan P and Jagannathan R 1997 *Phys. Chem. Glasses* **38** 59